

Experimental construction of generic three-qubit states and their reconstruction from two-party reduced states on an NMR quantum information processor

Shruti Dogra,^{*} Kavita Dorai,[†] and Arvind[‡]

*Department of Physical Sciences, Indian Institute of Science Education & Research (IISER) Mohali,
Sector 81 Mohali, Manauli PO 140306 Punjab India.*

We experimentally explore the state space of three qubits on an NMR quantum information processor. We construct a scheme to experimentally realize a canonical form for general three-qubit states up to single-qubit unitaries. This form involves a non-trivial combination of GHZ and W-type maximally entangled states of three qubits. The general circuit that we have constructed for the generic state reduces to those for GHZ and W states as special cases. The experimental construction of a generic state is carried out for a nontrivial set of parameters and the good fidelity of preparation is confirmed by complete state tomography. The GHZ and W-states are constructed as special cases of the general experimental scheme. Further, we experimentally demonstrate a curious fact about three-qubit states, where for almost all pure states, the two-qubit reduced states can be used to reconstruct the full three-qubit state. For the case of a generic state and for the W-state, we demonstrate this method of reconstruction by comparing it with the directly tomographed three-qubit state.

PACS numbers: 03.67.Lx, 03.67.Bg

I. INTRODUCTION

While a qubit is considered to be a building block for quantum information processing, the actual quantum computer invariably involves complex states of multiple qubits [1]. The transition from one to two qubits is of fundamental importance because it is the two-qubit system for which we can have entangled states and hence a nontrivial quantum advantage for information processing [2, 3]. The manipulation of two-qubit states is qualitatively more difficult than that for a single qubit. As a matter of fact, the dynamics of a single qubit finds a classical analog in polarization optics [4], and it is only when we create entangled states of two qubits, do the nontrivial quantum aspects emerge [5]. It may appear that moving from two qubits to several qubits is merely a matter of detail. However, this is not the case and new quantum aspects emerge for a three-qubit system, which is the simplest system for which the concept of multi-partite entanglement can be introduced. Unlike the two-qubit case, the maximally entangled states of three qubits are not equivalent up to local unitary transformations and instead fall into two inequivalent classes, namely the GHZ and W classes of states [6]. In contradistinction to the two-qubit case, a canonical form for three qubits turns out to be nontrivial and involves a combination of GHZ and W states. It has been shown that all pure states of a system of three qubits are equivalent under local unitary transformations to a canonical state with five independent non-zero real parameters [7–11]. While one-qubit reduced states have information

about the amount of entanglement in a two-qubit pure state, they do not uniquely determine the state. On the other hand, it turns out that almost every three-qubit pure state is completely determined by its two-qubit reduced density matrices and there is no more information in the full quantum state than what is already contained in the three possible two-qubit reduced states [12–14]. It is indeed somewhat surprising that even when nontrivial multi-partite entanglement is present, the “parts” can determine the “whole”.

There have been several experimental implementations of tripartite-entangled W and GHZ states using different physical resources [15–19]. GHZ and W states have been used as a resource in a quantum prisoner’s dilemma game [20], to simulate the violation of Bell-type inequalities [21], in quantum erasers [22, 23] and complementarity measurements [24], quantum key distribution [25], quantum secret sharing [26] and quantum teleportation [27]. In the context of NMR quantum computing, GHZ and W states have been generated on a one-dimensional Ising chain [28, 29], their decoherence properties studied [30], and their ground state phase transitions investigated in a system with competing many-body interactions [31, 32].

This work has two main results: (a) We prescribe a scheme to create generic states of three qubits and implement it on an NMR quantum computer. The complete class of separable, biseparable and maximally entangled three-qubit states can be generated using our scheme; (b) We experimentally demonstrate the reconstruction of generic three-qubit states from their two-qubit reduced marginals. The material in this paper is organized as follows: Section II describes the NMR implementation of a generic state with a nontrivial five-parameter set, and the implementations of the GHZ and W-states as special cases of the general scheme. The density matrices of all the states are reconstructed by using an optimal set of NMR state tomography experiments. Section III

^{*} shrutidogra@iisermohali.ac.in

[†] kavita@iisermohali.ac.in

[‡] arvind@iisermohali.ac.in

describes the three-qubit state reconstruction from their two-party reduced states for a generic state and for the W-state. By comparing the state tomographs obtained from the two-qubit marginals and by a full tomography of the three-qubit state we demonstrate that, reduced two-qubit density matrices are indeed able to capture all information about the full three-qubit state. Section IV contains some concluding remarks.

II. NMR IMPLEMENTATION

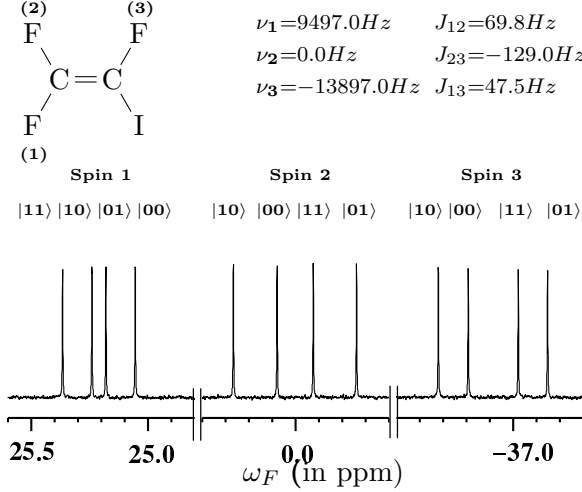


FIG. 1. Molecular structure, NMR parameters and ^{19}F thermal equilibrium spectrum of trifluoriodoethylene. The three fluorine spins in the molecule are marked as the corresponding qubits. The table summarizes the relevant NMR parameters i.e. resonance frequencies ν_i and J-coupling constants. The ^{19}F spectrum is obtained after a $\pi/2$ readout pulse on the thermal equilibrium state. The resonance lines of each qubit are labeled by the corresponding logical states of the other two qubits in the computational basis.

The three-qubit system that we use for NMR quantum information processing is the molecule trifluoriodoethylene dissolved in deuterated acetone. The three qubits were encoded using the ^{19}F nuclei. The Hamiltonian of the three-qubit system in the rotating frame is given by

$$H = \sum_{i=1}^3 \nu_i I_{iz} + \sum_{i<j, i=1}^3 J_{ij} I_{iz} I_{jz} \quad (1)$$

where I_{iz} is the single-spin Pauli angular momentum operator, ν_i are the Larmor frequencies of the spins and J_{ij} are the spin-spin coupling constants. The coupling constants recorded are $J_{12} = 69.8$ Hz, $J_{23} = -129.0$ Hz, and $J_{13} = 47.5$ Hz. Decoherence is not a major issue in this system, with average fluorine longitudinal T_1 relaxation times of 5.0 seconds and T_2 relaxation times of 1.0 seconds respectively. The structure of the three-qubit molecule as well as the equilibrium NMR spectrum obtained after a $\pi/2$ readout pulse are shown in Fig. 1.

The resonance lines of each qubit are labeled by the corresponding states of the other two coupled qubits. All experiments were performed at room temperature on a Bruker Avance III 400 MHz NMR spectrometer equipped with a z-gradient BBO probe. The three fluorine nuclei cover a very large bandwidth of 68 ppm. Standard shaped pulses (of duration $400\mu\text{s}$) were hence modulated to achieve uniform excitation of all the three qubits by exciting smaller bandwidths simultaneously at different offsets. Individual qubits were addressed using low power 'Gaussian' shaped selective pulses of $265\mu\text{s}$ duration. Before implementing the entangling circuits, the system was first initialized into the $|000\rangle$ pseudopure state by the spatial averaging technique [33], with the density operator given by

$$\rho_{000} = \frac{1-\epsilon}{8} I_8 + \epsilon |000\rangle\langle 000| \quad (2)$$

with a thermal polarization $\epsilon \approx 10^{-5}$ and I_8 being an 8×8 identity matrix. The experimentally created pseudopure state $|000\rangle$ was tomographed with a fidelity of 0.99. All experimentally generated states were completely characterized by performing NMR state tomography [34]. A modified tomographic protocol has been proposed [35], wherein a set of 7 operations defined by $\{\text{III}, \text{XXX}, \text{IIY}, \text{XYX}, \text{YII}, \text{XXY}, \text{IYY}\}$ is performed on the system before recording the signal. Here $X(Y)$ denotes a single spin operator and I is the identity operator. These operators can be implemented by applying the corresponding spin selective $\pi/2$ pulses. Motivated by this modified tomographic protocol, we used an expanded set of 11 operations defined by $\{\text{III}, \text{IIX}, \text{IXI}, \text{XII}, \text{IYY}, \text{IYI}, \text{YII}, \text{YYI}, \text{IXX}, \text{XXX}, \text{YYY}\}$ to determine all the 63 variables for our system of three qubits. We needed a slightly expanded set in order to perform experimentally accessible measurements that were sufficient to completely characterize the experimental density matrix with good fidelity. As a measure of the fidelity of the experimentally reconstructed density matrices, we use [36]:

$$F = \frac{\text{Tr}(\rho_{\text{theory}}^\dagger \rho_{\text{expt}})}{\sqrt{\text{Tr}(\rho_{\text{theory}}^\dagger \rho_{\text{theory}})} \sqrt{\text{Tr}(\rho_{\text{expt}}^\dagger \rho_{\text{expt}})}} \quad (3)$$

where ρ_{theory} and ρ_{expt} denote the theoretical and experimental density matrices respectively.

A. Generic state implementation

The canonical (generic) state for three qubits proposed in [7] is given by:

$$|\psi\rangle = a_1|000\rangle + a_2|001\rangle + a_3|010\rangle + a_4|100\rangle + a_5 e^{i\phi}|111\rangle \quad (4)$$

$a_i \geq 0; \quad \sum_i a_i^2 = 1$

The normalization condition leads to reduction of one parameter and hence the state has five independent non-zero, real parameters (four moduli and one phase). The

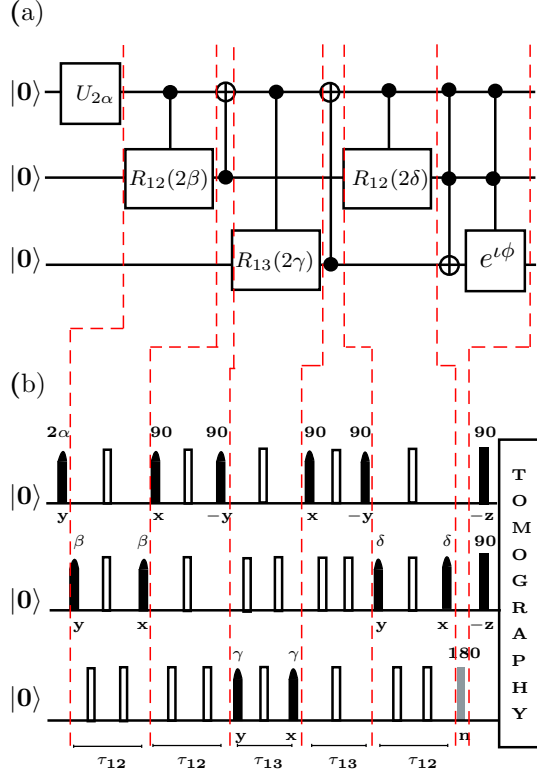


FIG. 2. (Color online) (a) Quantum circuit showing the specific sequence of implementation of the controlled-rotation, controlled-NOT, controlled-controlled-NOT and controlled-controlled-phase gates required to construct a generic state and (b) NMR pulse sequence to implement a general three-qubit generic state; τ_{ij} is the evolution period under the J_{ij} coupling. The 180° pulses are represented by unfilled rectangles. The other pulses are labeled with their specific flip angles and phases. The last pulse (gray shaded) on the third qubit is a transition-selective 180° pulse on the $|110\rangle$ to $|111\rangle$ transition about an arbitrary axis \hat{n} which is inclined at angle $(\phi + 90)$ with the x -axis. The last two rectangular pulses on the first and second qubits are 90° z -rotations, to compensate the extra phases acquired (as described in the text).

state is symmetric under permutations of the qubits and the five components which are invariant under local unitaries (single-qubit operations) are the minimal number of non-local parameters required to completely specify the state. Any three-qubit state up to local unitaries, can hence be written in the form given in Eqn. (4). We base our experimental construction on this canonical form and will henceforth refer to it as the generic three-qubit state. The generic three-qubit state can be constructed by a sequence of gates, starting from the system in a pseudopure state. These gates are one-parameter unitary transformations and as will be shown, have elegant decompositions in terms of NMR pulses. The normalization condition is automatically satisfied as the normalization will be preserved under these unitary operations.

The sequence of gates with four real parameters $\alpha, \beta, \gamma, \delta$ representing the amplitude parameters $a_1 \dots a_5$

and the phase ϕ leading to the construction of a generic three-qubit state is detailed below:

$$\begin{aligned}
 |000\rangle &\xrightarrow{U_{2\alpha}} \cos \alpha |000\rangle + \sin \alpha |100\rangle \\
 \text{CROT}_{12}^{2\beta} &\xrightarrow{\quad} \cos \alpha |000\rangle + \sin \alpha \cos \beta |100\rangle + \sin \alpha \sin \beta |110\rangle \\
 \text{CNOT}_{21} &\xrightarrow{\quad} \cos \alpha |000\rangle + \sin \alpha \cos \beta |100\rangle + \sin \alpha \sin \beta |010\rangle \\
 \text{CROT}_{13}^{2\gamma} &\xrightarrow{\quad} \cos \alpha |000\rangle + \sin \alpha \cos \beta \cos \gamma |100\rangle \\
 &\quad + \sin \alpha \cos \beta \sin \gamma |101\rangle + \sin \alpha \sin \beta |010\rangle \\
 \text{CNOT}_{31} &\xrightarrow{\quad} \cos \alpha |000\rangle + \sin \alpha \cos \beta \cos \gamma |100\rangle \\
 &\quad + \sin \alpha \cos \beta \sin \gamma |001\rangle + \sin \alpha \sin \beta |010\rangle \\
 \text{CROT}_{12}^{2\delta} &\xrightarrow{\quad} \cos \alpha |000\rangle + \sin \alpha \cos \beta \cos \gamma \cos \delta |100\rangle \\
 &\quad + \sin \alpha \cos \beta \cos \gamma \sin \delta |110\rangle \\
 &\quad + \sin \alpha \cos \beta \sin \gamma |001\rangle + \sin \alpha \sin \beta |010\rangle \\
 \text{CCN}_{12,3} &\xrightarrow{\quad} \cos \alpha |000\rangle + \sin \alpha \cos \beta \cos \gamma \cos \delta |100\rangle \\
 &\quad + \sin \alpha \cos \beta \cos \gamma \sin \delta |111\rangle \\
 &\quad + \sin \alpha \cos \beta \sin \gamma |001\rangle + \sin \alpha \sin \beta |010\rangle \\
 \text{Ph}_{12,3}^\phi &\xrightarrow{\quad} \cos \alpha |000\rangle + \sin \alpha \cos \beta \sin \gamma |001\rangle \\
 &\quad + \sin \alpha \sin \beta |010\rangle + \sin \alpha \cos \beta \cos \gamma \cos \delta |100\rangle \\
 &\quad + e^{i\phi} \sin \alpha \cos \beta \cos \gamma \sin \delta |111\rangle
 \end{aligned} \tag{5}$$

The operator $U_{2\alpha}^1$ is a separable, non-entangling transformation belonging to the $SU(2)$ group which implements a rotation by an arbitrary angle α on the first qubit, leading to a generalized superposition state of the qubit. The global phase is not detectable in NMR experiments and is thus ignored throughout in gate implementation; $\text{CROT}_{ij}^{2\theta}$ implements a controlled rotation by an arbitrary angle θ , with the i^{th} qubit as control and j^{th} as target; CNOT_{ij} implements a controlled-NOT gate, with the i^{th} qubit as control and j^{th} as target; $\text{CCN}_{12,3}$ implements a controlled-controlled-NOT (Toffoli) gate on the 3rd qubit i.e. it flips the state of qubit 3, if and only if both qubits 1 and 2 are in the $|1\rangle$ state; $\text{Ph}_{12,3}^\phi$ is a controlled-controlled-phase shift gate with 1,2 as control qubits and 3 being the target qubit. The state thus obtained has five variables: $\alpha \in [0, \pi/2]$, $\beta \in [0, \pi/2]$, $\gamma \in [0, \pi/2]$, $\delta \in [0, \pi/2]$ and $\phi \in [0, 2\pi]$.

The quantum circuit for generic state construction is given in Fig. 2(a). The circuit consists of a single-qubit rotation gate, followed by several two-qubit controlled-rotation and controlled-NOT gates, a three-qubit controlled-controlled NOT (Toffoli) gate, and finally a controlled-controlled phase gate that introduces a relative phase in the $|111\rangle$ state.

The NMR pulse sequence to construct the generic three-qubit state starting from the pseudopure state $|000\rangle$ is given in Fig. 2(b). Refocusing pulses are used in the middle of all J-evolution periods to compensate for chemical shift evolution. Pairs of π pulses have

been inserted at 1/4 and 3/4 of the J-evolution intervals to eliminate undesirable evolution due to other J-couplings. The 180° pulses are represented by unfilled rectangles, while the other pulses are labeled with their specific flip angles and phases. An ideal controlled rotation gate CROT_{ij} , where ‘i’ is control and ‘j’ is the target qubit ($i < j$) is implemented by the sequence: $(\theta)_{-y}^j (\frac{\pi}{2})_z^{i,j} \frac{1}{4J_{ij}} (\pi)_y^{i,j} \frac{1}{4J_{ij}} (\pi)_y^{i,j} (\theta)_{-y}^j (\pi)_z^{i,j}$ [39]; here $(\theta)_\alpha^i$ denotes an rf pulse of flip angle θ and phase α applied on the i th qubit, $(\beta)_\alpha^{i,j}$ denotes an rf pulse of flip angle β and phase α applied simultaneously on both the i th and j th qubits, and $\frac{1}{4J_{ij}}$ denotes an evolution period under the coupling Hamiltonian (using standard NMR notation). The above sequence for the ideal CROT_{ij} gate contains two z -rotations on each of the control and target qubits, which are of long duration and give rise to experimental imperfections. In order to shorten the gate duration and hence reduce experimental artifacts, we implemented a shorter pulse sequence corresponding to $(\theta)_{-y}^j \frac{1}{4J_{ij}} (\pi)_y^{i,j} \frac{1}{4J_{ij}} (\pi)_y^{i,j} (\theta)_{-x}^j$, which creates the desired state alongwith a relative phase. We keep track of the relative phase gained at the end of each controlled operation and implement z -rotations on the spins at the end of the sequence to compensate for the relative phases acquired. The last two gates in the circuit, namely the controlled-controlled NOT (Toffoli) gate and the controlled-controlled phase gate were simultaneously implemented using a single transition-selective π pulse, applied about an arbitrary axis of rotation $\hat{\mathbf{n}}$ (gray-shaded in Fig. 2(b)) [37, 38]. A three-qubit controlled-controlled NOT (Toffoli) gate can be experimentally realized by a transition-selective $(\pi)_y$ pulse between energy levels $|110\rangle$ and $|111\rangle$. A transition-selective pulse $(\pi)_{\hat{\mathbf{n}}}$ about an arbitrary axis of rotation $\hat{\mathbf{n}} = \cos \phi' \hat{\mathbf{x}} + \sin \phi' \hat{\mathbf{y}}$, on the other hand, introduces an extra phase of $e^{i\phi}$ ($\phi' = \phi + \pi/2$). Hence, $(\pi)_{\hat{\mathbf{n}}}^{(110) \rightarrow (111)}$ when applied on the basis vector $|110\rangle$, results in the state $e^{i\phi}|111\rangle$. This is an ingenious method to reduce the experimental time, and comes in handy in completing the circuit implementation before the decoherence begins to introduce significant distortions.

To demonstrate our general method to create generic three-qubit states, we implement our scheme to create a state with a nontrivial structure. We chose a state in which all the terms in the generic state expression given in Eqn. 5 are involved in a nontrivial way. We have chosen $\alpha = 45^\circ, \beta = 55^\circ, \gamma = 60^\circ, \delta = 58^\circ$ and $\phi = 125^\circ$. This set of parameters leads to the creation of the generic state:

$$0.707|000\rangle + 0.351|001\rangle + 0.579|010\rangle + 0.107|100\rangle + 0.172e^{i(125^\circ)}|111\rangle \quad (6)$$

The tomograph corresponding to this state is shown in Fig. 3, wherein the experimentally tomographed state (Fig. 3(b)) is compared with the theoretically expected state (Fig. 3(a)). The fidelity of the experimentally to-

mographed state (by the definition given in Eqn. 3) in th

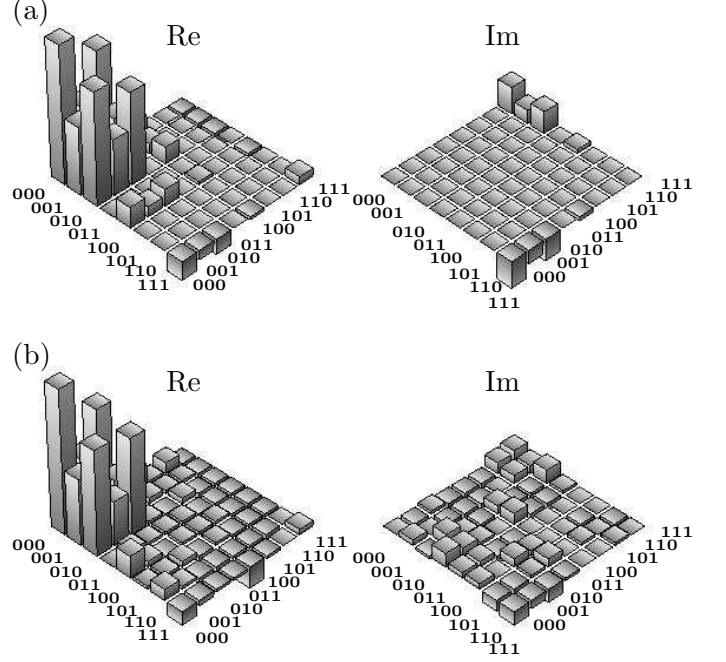


FIG. 3. The real (Re) and imaginary (Im) parts of the (a) theoretical and (b) experimental density matrices for the three-qubit generic state, reconstructed using full state tomography. The values of the parameters are $\alpha = 45^\circ, \beta = 55^\circ, \gamma = 60^\circ, \delta = 58^\circ, \phi = 125^\circ$. The rows and columns encode the computational basis in binary order, from $|000\rangle$ to $|111\rangle$. The experimentally tomographed state has a fidelity of 0.92.

Our method is quite general and can be used to construct any generic state of the three-qubit system. Given that the relaxation times for our system are quite long and the qubits are well separated in frequency space, it is also possible to perform single-qubit operations to transform the state further.

B. GHZ state implementation

Generalized GHZ states are a special case of the generic state given in Eqn. 4, corresponding to the parameter values $\alpha = \alpha, \beta = \gamma = 0, \delta = \pi/2, \phi = 0$, and the circuit given in Fig. 2(a) reduces to the circuit given in Fig. 4(a). The two controlled-rotation gates $\text{CROT}_{12}^{2\beta}$ and $\text{CROT}_{13}^{2\gamma}$ are hence redundant for the state implementation and the simplified experimental circuit is given in Fig. 4(b), with a single-qubit rotation followed by two controlled-NOT gates. An arbitrarily weighted GHZ kind of entangled state can be prepared from the initial pseudopure state $|000\rangle$ by the sequence of operations

$$|000\rangle \xrightarrow{U_{2\alpha}^1} \cos \alpha |000\rangle + \sin \alpha |100\rangle \xrightarrow{\text{CNOT}_{12}} \cos \alpha |000\rangle + \sin \alpha |110\rangle$$

$$\xrightarrow{\text{CNOT}_{13}} \cos \alpha |000\rangle + \sin \alpha |111\rangle \quad (7)$$

For $\alpha = \pi/4$, the above sequence leads to a pure GHZ state [15, 16, 23]:

$$|\psi_{\text{GHZ}}\rangle = \frac{1}{\sqrt{2}}(|000\rangle + |111\rangle) \quad (8)$$

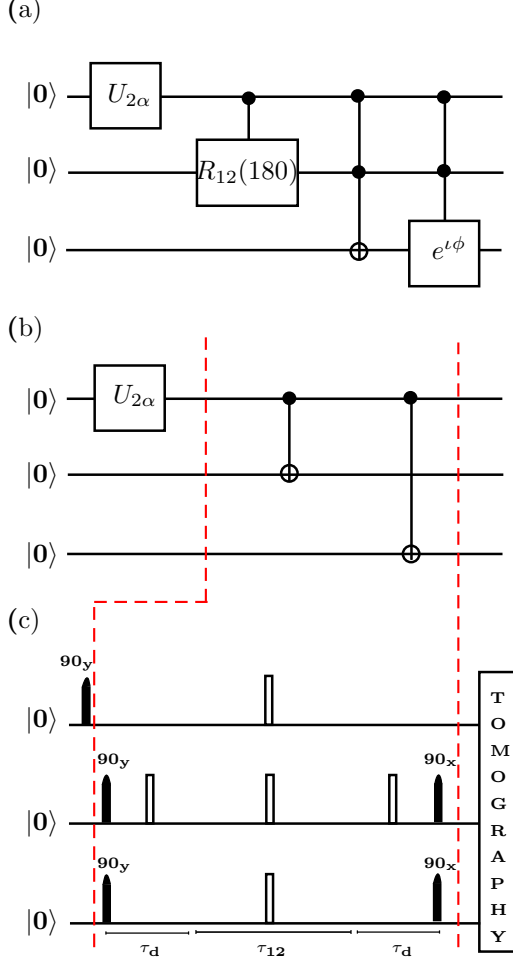


FIG. 4. (Color online) (a) Quantum circuit to implement a generalized GHZ state, derived from the general circuit for generic state construction given in Fig. 2(a). (b) Simplified circuit for experimental implementation of the GHZ state. (c) NMR pulse sequence corresponding to the circuit in (b). The $\tau_d = \frac{\tau_{13} - \tau_{12}}{2}$ period is tailored such that the system evolves solely under the J_{13} coupling term.

The quantum circuit and the NMR pulse sequence used to create an arbitrary GHZ-like entangled state beginning from the pseudopure state $|000\rangle$ and ignoring overall phase factors are given in Fig. 4(b) and (c) respectively. The CNOT_{12} and CNOT_{13} in the circuit are controlled-NOT gates with qubit 1 as the control and qubit 2 (3) as the target. Since the target qubits are different in both these cases, these gates commute and can be applied in parallel, leading to a reduction in experimental time. For our system $\tau_{13} > \tau_{12}$, where τ_{ij} denotes the

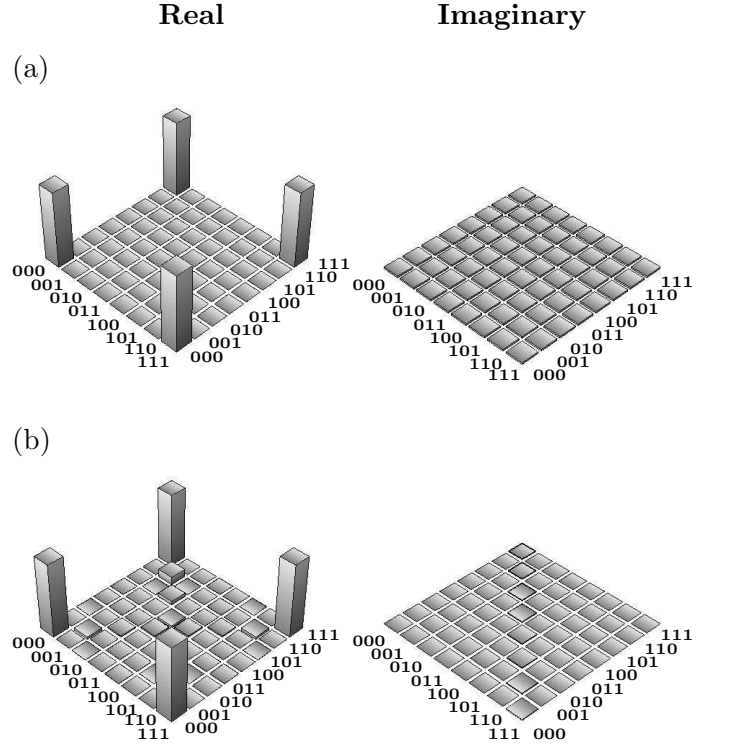


FIG. 5. The real (Re) and imaginary (Im) parts of the (a) theoretical and (b) experimental density matrices for the GHZ state, reconstructed using full state tomography. The rows and columns encode the computational basis in binary order, from $|000\rangle$ to $|111\rangle$. The experimentally tomographed state has a fidelity of 0.97.

evolution period under the $\frac{1}{2J_{ij}}$ coupling term. Hence, during the period τ_{12} , both qubits 2 and 3 evolve under the the J-couplings J_{12} and J_{13} (Fig. 4(c)). The evolution in the intervals $\tau_d = \frac{\tau_{13} - \tau_{12}}{2}$ is solely governed by the J_{13} coupling term, and by the end of the evolution period, the system evolves under J_{12} and J_{13} couplings for durations $\frac{1}{2J_{12}}$ and $\frac{1}{2J_{13}}$ respectively. The state generated experimentally (Fig. 5(b)) was tomographed and lies very close to the theoretically expected state (Fig. 5(a)) with a computed fidelity of 0.97.

C. W-state implementation

Generalized W-states are another special case of the generic state given in Eqn. 4, corresponding to the parameter values $\alpha = \pi/2, \beta, \gamma \in [0, \pi/2], \delta = 0, \phi = 0$, leading to the state $|\psi\rangle = \cos \gamma \cos \beta |100\rangle + \sin \gamma \cos \beta |001\rangle + \sin \beta |010\rangle$. The circuit for generalized W-states derived from the circuit in Fig. 2(a) is given in Fig. 6(a) and can be constructed by the sequential operation of the gates:

$$|000\rangle \xrightarrow{U_{\pi}^1} |100\rangle$$

$$\begin{aligned}
& \xrightarrow{\text{CROT}_{12}^{2\beta}} \cos \beta |100\rangle + \sin \beta |110\rangle \\
& \xrightarrow{\text{CNOT}_{21}} \cos \beta |100\rangle + \sin \beta |010\rangle \\
& \xrightarrow{\text{CROT}_{13}^{2\gamma}} \cos \gamma \cos \beta |100\rangle + \sin \gamma \cos \beta |101\rangle + \sin \beta |010\rangle \\
& \xrightarrow{\text{CNOT}_{31}} \cos \gamma \cos \beta |100\rangle + \sin \gamma \cos \beta |001\rangle + \sin \beta |010\rangle
\end{aligned} \tag{9}$$

The first gate in the circuit, namely a rotation by π on the first qubit, can be avoided by starting the implementation on a different initial state. We hence begin with the pseudopure state $|100\rangle$ as the initial state in our experiments. We also avoid implementing the second gate in the circuit in Eqn. (9), namely the controlled-rotation $\text{CROT}_{12}^{2\beta}$ gate, and instead implement the much simpler $U_{2\beta}^2$ gate on the second qubit, which in this case yields the same result. For $2\beta = 2 \sin^{-1}(1/\sqrt{3})$ and $\gamma = 45^\circ$, the circuit leads to implementation of the standard W-state upto a phase factor

$$|\psi_W\rangle = \frac{1}{\sqrt{3}}(i|001\rangle + |010\rangle + |100\rangle) \tag{10}$$

One can get rid of the extra phase factor by a single-qubit unitary gate. The simplified experimental circuit and the NMR pulse sequence for the creation of an arbitrary W-like entangled state beginning from the pseudopure state $|100\rangle$ and ignoring overall phase factors, are given in Figs. 6(b) and (c) respectively. The experimentally reconstructed density matrix (Fig. 7(b)) matches well with the theoretically expected values (Fig. 7(a)), with a computed state fidelity of 0.96.

III. THREE-QUBIT STATE RECONSTRUCTION FROM TWO-PARTY REDUCED STATES

Linden et al. discovered a surprising fact about multiparty correlations, namely, that “the parts determine the whole for a generic pure state” [12, 40]. For three qubits, this implies that all the information in a generic three-party state is contained in its three two-party reduced states, which then uniquely determine the full three-party state. The only exceptions to the above hypothesis are the generalized GHZ states, and no set of their reduced states can uniquely determine such entangled states. This is an important result which sheds some light on how information is stored in multipartite entangled states. In a related work, Diosi et al. [13] presented a tomographic protocol to completely characterize almost all generic three-qubit pure states, based only on pairwise two-qubit detectors.

In this paper we describe the first experimental demonstration of this interesting quantum mechanical feature of three-qubit states. We use the same algorithm delineated by Diosi et al. [13], to reconstruct three-qubit states from their two-party reduced states. Let us consider a three-qubit pure state $\rho_{ABC} = |\psi_{ABC}\rangle\langle\psi_{ABC}|$, with ρ_{AB}, ρ_{BC} ,

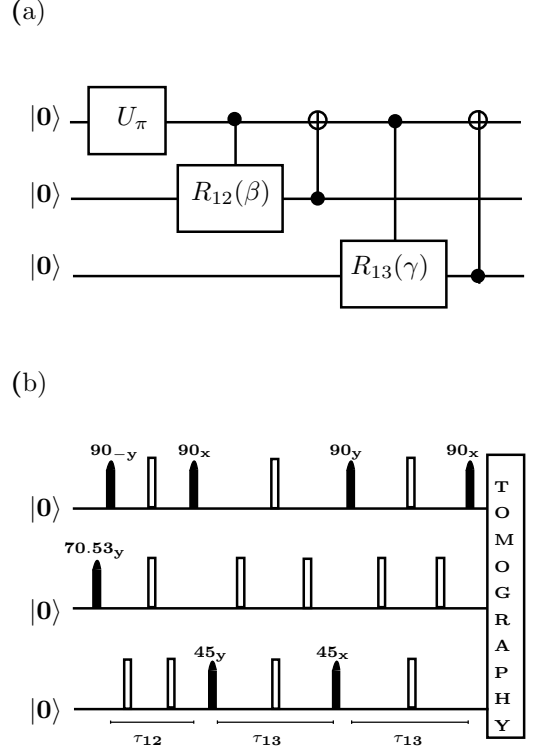


FIG. 6. (Color online) (a) Quantum circuit to implement the W-state, derived from the general circuit for generic state construction given in Fig. 2(a). (b) Simplified circuit for experimental implementation of the W-state. (c) NMR pulse sequence to experimentally implement the W-state, starting from the initial pseudopure state $|100\rangle$. The first pulse on the second qubit implements a $U_{2\beta}^2$ rotation, with $2\beta = 2 \sin^{-1}(1/\sqrt{3}) \equiv 70.53^\circ$.

ρ_{AC} being its two-party reduced states. The single-qubit reduced states ρ_A , ρ_B and ρ_C can be further obtained from the two-party reduced states. Since ρ_{ABC} is pure, ρ_A and ρ_{BC} share the same set of eigen values, and can be written as

$$\begin{aligned}
\rho_A &= \sum_i p_A^i |i\rangle\langle i| \\
\rho_{BC} &= \sum_i p_A^i |i; BC\rangle\langle i; BC|
\end{aligned} \tag{11}$$

where $\{|i\rangle\}$ are the eigenvectors of ρ_A with eigenvalues $\{p_A^i\}$, and $\{|i; BC\rangle\}$ are the eigenvectors of ρ_{BC} with eigenvalues $\{p_A^i\}$. The three-qubit states compatible with ρ_A and ρ_{BC} are

$$|\psi_{ABC}; \alpha\rangle = \sum_i e^{i\alpha_i} \sqrt{p_A^i} |i\rangle \otimes |i; BC\rangle \tag{12}$$

Using a similar argument, the set of three-qubit pure states obtained from ρ_{AB} and ρ_C is given by

$$|\psi_{ABC}; \gamma\rangle = \sum_k e^{i\gamma_k} \sqrt{p_C^k} |k; AB\rangle \otimes |k\rangle \tag{13}$$

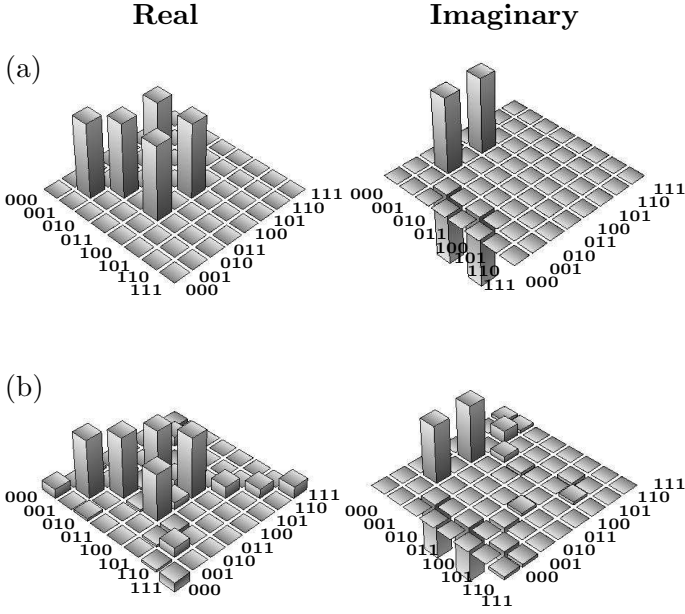


FIG. 7. The real (Re) and imaginary (Im) parts of the (a) theoretical and (b) experimental density matrices for the W state, reconstructed using full state tomography. The rows and columns encode the computational basis in binary order, from $|000\rangle$ to $|111\rangle$. The experimentally tomographed state has a fidelity of 0.96.

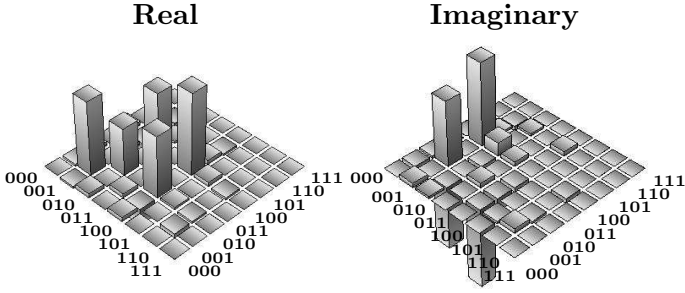


FIG. 8. The real (Re) and imaginary (Im) parts of the density matrix for the W-state: (a) The two-qubit reduced density matrix ρ_{AB} . (b) The two-qubit reduced density matrix ρ_{BC} . (c) The entire three-qubit density matrix ρ_{ABC} , reconstructed from the corresponding two-qubit reduced density matrices. The rows and columns encode the computational basis in binary order, from $|00\rangle$ to $|11\rangle$ for two qubits and from $|000\rangle$ to $|111\rangle$ for three qubits. The tomographed state has a fidelity of 0.97.

where $\{|k\rangle\}$ are the eigenvectors of ρ_C with eigenvalues $\{p_C^k\}$ and $\{|k; AB\rangle\}$ are the corresponding eigenvectors of ρ_{AB} . Since the pure state $|\psi_{ABC}\rangle$ is compatible with both ρ_{AB} and ρ_{BC} , we can determine the values of α_i and γ_k such that $|\psi_{ABC}; \alpha\rangle = |\psi_{ABC}; \gamma\rangle$. We thus obtain almost all three-qubit pure states from any two of their corresponding two-party reduced states. The set (ρ_{AB}, ρ_{AC}) or the equivalent set (ρ_{AB}, ρ_{BC}) can be used to reconstruct ρ_{ABC} .

The two-party reduced states ρ_{AB} , ρ_{BC} and ρ_{AC} were

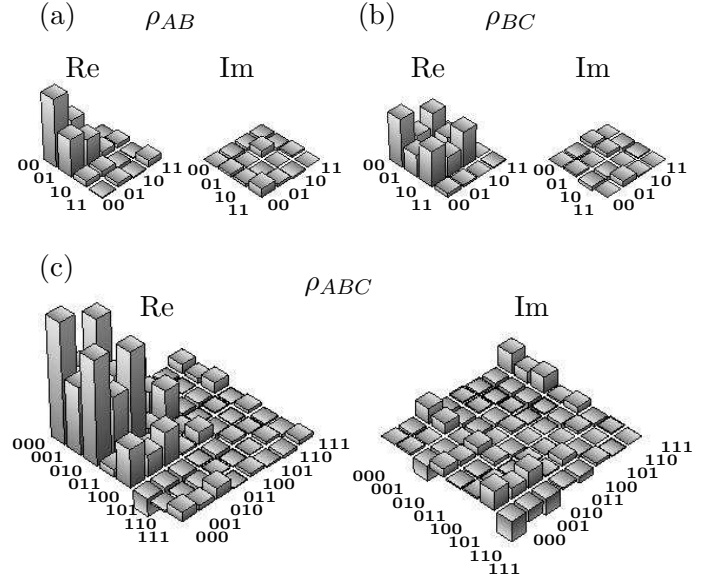


FIG. 9. The real (Re) and imaginary (Im) parts of the density matrix for the generic state: (a) The two-qubit reduced density matrix ρ_{AB} . (b) The two-qubit reduced density matrix ρ_{BC} . (c) The entire three-qubit density matrix ρ_{ABC} , reconstructed from the corresponding two-qubit reduced density matrices. The parameter set includes $\alpha = 45^\circ, \beta = 55^\circ, \gamma = 60^\circ, \delta = 58^\circ, \phi = 125^\circ$. The rows and columns encode the computational basis in binary order, from $|00\rangle$ to $|11\rangle$ for two qubits and from $|000\rangle$ to $|111\rangle$ for three qubits. The tomographed state has a fidelity of 0.90.

computed by performing partial state tomography. The set of tomography operations performed to experimentally reconstruct all three two-party reduced states include: $\{\text{III, IXI, IYI, XXI}\}$ to reconstruct ρ_{AB} ; $\{\text{III, IIX, IYY, IXX}\}$ to reconstruct ρ_{BC} and $\{\text{III, IIX, IYY, XIX}\}$ to reconstruct ρ_{AC} . Almost any three-qubit pure state ρ_{ABC} (except those belonging to the generalized GHZ class) can be determined by choosing any two sets from the above. The three-party state ρ_{ABC} reconstructed using the (ρ_{AB}, ρ_{BC}) set of two-party reduced states was compared with the same state reconstructed using complete tomography, and the results match well. For the W state we tomographed ρ_{AB} and ρ_{BC} to give us

$$\rho_{AB} = \begin{pmatrix} 0.36 & 0. & 0. & 0. - 0.01i \\ 0. & 0.21 & 0.2 + 0.05i & -0.01 \\ 0. & 0.2 - 0.05i & 0.21 & 0.01 \\ 0. + 0.01i & -0.01 & 0.01 & 0.22 \end{pmatrix}$$

$$\rho_{BC} = \begin{pmatrix} 0.34 & -0.01 & 0. + 0.01i & 0 \\ -0.01 & 0.3 & 0. + 0.24i & 0.02 \\ -0.01 & 0. - 0.24i & 0.2 & 0. \\ 0 & 0.02 & 0 & 0.16 \end{pmatrix} \quad (14)$$

These experimental tomographed density matrices were then used to reconstruct the three-qubit W-state density matrix ρ_{ABC} . The thus reconstructed ρ_{ABC} is given by

$$\rho_{ABC} = \begin{pmatrix} 0. & -0.01 - 0.02i & 0.02 - 0.01i & 0. & 0.02 & 0. & 0. & 0. \\ -0.01 + 0.02i & 0.36 & 0. + 0.29i & 0.02 & -0.1 + 0.37i & -0.01 + 0.01i & -0.02 - 0.02i & 0. \\ 0.02 + 0.01i & 0. - 0.29i & 0.23 & 0. - 0.02i & 0.3 + 0.08i & 0.01 & -0.01 + 0.01i & 0. \\ 0. & 0.02 & 0. + 0.02i & 0. & -0.01 + 0.02i & 0. & 0. & 0. \\ 0.02 & -0.1 - 0.37i & 0.3 - 0.08i & -0.01 - 0.02i & 0.4 & 0.02 & -0.01 + 0.02i & 0. \\ 0. & -0.01 - 0.01i & 0.01 & 0. & 0.02 & 0. & 0. & 0. \\ 0. & -0.02 + 0.02i & -0.01 - 0.01i & 0. & -0.01 - 0.02i & 0. & 0. & 0. \\ 0. & 0. & 0. & 0. & 0. & 0. & 0. & 0. \end{pmatrix} \quad (15)$$

The reconstructed density matrix for the W-state is shown in Fig. 8, computed from two sets of the corresponding two-qubit reduced density matrices. The tomographed state has a fidelity of 0.97, which matches well with the fidelity of the original three-qubit density matrix of the W-state (Fig. 7(b)). As another illustration of reconstructing the whole state from its parts, the reconstructed density matrix of the experimentally generated generic state with a parameter set: $\alpha = 45^\circ, \beta = 55^\circ, \gamma = 60^\circ, \delta = 58^\circ, \phi = 125^\circ$, is shown in Fig. 9. The two-party reduced states were able to reconstruct this three-qubit state with a fidelity of 0.90, which compares well with the full reconstruction of the entire three-qubit state given in Fig. 3(b).

IV. CONCLUDING REMARKS

We have proposed and implemented an NMR-based scheme to construct a generic three-qubit state from which any general pure state of three-qubits (including separable, biseparable and maximally entangled states) can be constructed, up to local unitaries. Full tomographic reconstruction of the experimentally generated

states showed good fidelity of preparation and we have achieved a high degree of control over the state space of three-qubit quantum systems. Generating generic three-qubit states with a nontrivial phase parameter was an experimental challenge and we archived it by crafting a special pulse scheme. It has been previously shown that in a system of three qubits, no irreducible three-party correlations exist and that all information about the full quantum state is completely contained in the three two-party correlations. We have demonstrated this important result experimentally in a system of three qubits. The three-qubit density operator ρ_{ABC} is obtained by complete quantum state tomography and compared with the same three-qubit state reconstructed from tomographs of the two-party reduced density operators given by ρ_{AB} , ρ_{BC} and ρ_{AC} . It is expected that our experiments will pave the way for an understanding of how information is stored in multi-partite entangled systems.

ACKNOWLEDGMENTS

All experiments were performed on a Bruker Avance-III 400 MHz FT-NMR spectrometer at the NMR Research Facility at IISER Mohali. SD acknowledges UGC India for financial support.

-
- [1] M. A. Nielsen and I. L. Chuang, *Quantum Computation and Quantum Information* (Cambridge University Press, Cambridge UK, 2000).
 - [2] R. Horodecki, P. Horodecki, M. Horodecki, and K. Horodecki, *Rev. Mod. Phys.* **81**, 865 (2009).
 - [3] T. D. Ladd, F. Jelezko, R. Laflamme, Y. Nakamura, C. Monroe, and J. L. O'Brien, *Nature* **464**, 45 (2010).
 - [4] Arvind, G. Kaur, and G. Narang, *J. Opt. Soc. Am. B* **24**, 221 (2007).
 - [5] W. K. Wootters, *Phys. Rev. Lett.* **80**, 2245 (1998).
 - [6] L. Chen and Y. X. Chen, *Phys. Rev. A* **74**, 062310 (2006).
 - [7] A. Acin, A. Andrianov, L. Costa, E. Jane, J. I. Latorre, and R. Tarrach, *Phys. Rev. Lett.* **85**, 1560 (2000).
 - [8] H. A. Carteret, A. Higuchi, and A. Sudbery, *J. Math. Phys.* **41**, 7932 (2000).
 - [9] A. Acin, D. Bruss, M. Lewenstein, and A. Sanpera, *Phys. Rev. Lett.* **87**, 040401 (2001).
 - [10] J. I. de Vicente, T. Carle, C. Streitberger, and B. Kraus, *Phys. Rev. Lett.* **108**, 060501 (2012).
 - [11] T. Vertesi, W. Laskowski, and K. F. Pal, *Phys. Rev. A* **89**, 012115 (2014).
 - [12] N. Linden, S. Popescu, and W. K. Wootters, *Phys. Rev. Lett.* **89**, 207901 (2002).
 - [13] L. Diosi, *Phys. Rev. A* **70**, 010302 (2004).
 - [14] D. Cavalcanti, L. M. Cioletti, and M. O. T. Cunha, *Phys. Rev. A* **71**, 014301 (2005).
 - [15] R. Laflamme, E. Knill, W. H. Zurek, P. Catasti, and S. V. S. Mariappan, *Proc. Roy. Soc. A* **356**, 1941 (1998).
 - [16] R. J. Nelson, D. G. Cory, and S. Lloyd, *Phys. Rev. A* **61**, 022106 (2000).
 - [17] H. Mikami, Y. Li, K. Fukuoka, and T. Kobayashi, *Phys. Rev. Lett.* **95**, 150404 (2005).
 - [18] K. J. Resch, P. Walther, and A. Zeilinger, *Phys. Rev. Lett.* **94**, 070402 (2005).
 - [19] C. F. Roos, M. Riebe, H. Haffner, W. Hansel, J. Benhelm, G. P. T. Lancaster, C. Becher, F. Schmidt-Kaler, and R. Blatt, *Science* **304**, 1478 (2004).
 - [20] Y. J. Han, Y. S. Zhang, and G. C. Guo, *Phys. Lett. A* **295**, 61 (2002).
 - [21] C. Ren, D. Lu, M. Shi, X. Peng, and J. Du, *Phys. Lett. A* **373**, 4222 (2009).

- [22] G. Teklemariam, E. M. Fortunato, M. A. Pravia, T. F. Havel, and D. G. Cory, *Chaos, Solitons and Fractals* **16**, 457 (2003).
- [23] G. Teklemariam, E. M. Fortunato, M. A. Pravia, Y. Sharf, T. F. Havel, D. G. Cory, A. Bhattacharyya, and J. Hou, *Phys. Rev. A* **66**, 012309 (2002).
- [24] X. Peng, J. Zhang, J. Du, and D. Suter, *Phys. Rev. A* **77**, 052107 (2008).
- [25] J. Kempe, *Phys. Rev. A* **60**, 910 (1999).
- [26] M. Hillery, V. Buzek, and A. Berthiaume, *Phys. Rev. A* **59**, 1829 (1999).
- [27] Y. Yeo and W. K. Chua, *Phys. Rev. Lett.* **96**, 060502 (2006).
- [28] K. R. K. Rao and A. Kumar, *Int. J. Qtm. Inf.* **4**, 1250039 (2012).
- [29] Y. Gao, H. Zhou, D. Zou, X. Peng, and J. Du, *Phys. Rev. A* **87**, 032335 (2013).
- [30] M. Kawamura, T. Morimoto, Y. Mori, R. Sawae, K. Takarabe, and Y. Manmoto, *Int. J. Qtm. Chem.* **106**, 3108 (2006).
- [31] X. Peng, J. Zhang, J. Du, and D. Suter, *Phys. Rev. Lett.* **103**, 140501 (2009).
- [32] X. Peng, J. Zhang, J. Du, and D. Suter, *Phys. Rev. A* **81**, 042327 (2010).
- [33] D. Cory, M. Price, and T. Havel, *Physica D* **120**, 82 (1998).
- [34] I. L. Chuang, N. Gershenfeld, M. Kubinec, and D. W. Leung, *Proc. Roy. Soc. A* **454**, 447 (1998).
- [35] G. M. Leskowitz and L. J. Mueller, *Phys. Rev. A* **69**, 052302 (2004).
- [36] Y. S. Weinstein, M. A. Pravia, E. M. Fortunato, S. Lloyd, and D. G. Cory, *Phys. Rev. Lett.* **86**, 1889 (2001).
- [37] K. Dorai and A. Kumar, *J. Magn. Reson.* **114 A**, 155 (1995).
- [38] X. Peng, X. Zhu, X. Fang, M. Feng, K. Gao, X. Yang, and M. Liu, *Chem. Phys. Lett.* **340**, 509 (2001).
- [39] J. A. Jones, R. Hansen, and M. Mosca, *J. Magn. Reson.* **135**, 353 (1998).
- [40] N. Linden and W. K. Wootters, *Phys. Rev. Lett.* **89**, 277906 (2002).